Strong Coupling of a Gd^{3+} Multilevel Spin System to an On-Chip Superconducting Resonator

Giovanni Franco-Rivera,[1,*] Josiah Cochran,[1] Seiji Miyashita,[2] Sylvain Bertaina,[3] and Irinel Chiorescu[1,†]

[1] *Department of Physics and The National High Magnetic Field Laboratory, Florida State University, Tallahassee, Florida 32310, USA*

[2] *Department of Physics, Graduate School of Science, The University of Tokyo, 7-3-1 Bunkyo-Ku, Tokyo 113-0033, Japan*

[3] *CNRS, Aix-Marseille Université, IM2NP (UMR 7344), Institut Matériaux Microélectronique et Nanosciences de Provence, Marseille, France*

(Received 21 August 2022; revised 7 October 2022; accepted 13 January 2023; published 24 February 2023)

We report the realization of a strong coupling between a Gd^{3+} spin ensemble hosted in a scheelite ($CaWO_4$) single crystal and the resonant mode of a coplanar-strip-line superconducting cavity leading to a large separation of spin-photon states of 146 MHz. The interaction is well described by the Dicke model and the crystal-field Hamiltonian of the multilevel spin system. We observe a change of the crystal-field parameters due to the presence of photons in the cavity, which generates a significant perturbation of the crystal ground state. Using finite-element calculations, we numerically estimate the cavity sensing volume as well as the average spin-photon coupling strength of $g_0/2\pi \approx 620$ Hz. Lastly, the dynamics of the spin-cavity states are explored via pulsed measurements by recording the cavity ring-down signal as a function of the pulse length and the amplitude. The results indicate a potential method to initialize this multilevel system in its ground state via an active cooling process.

DOI: 10.1103/PhysRevApplied.19.024067

I. INTRODUCTION

Interactions between quantum systems via electromagnetic excitations are currently the basis of operation of many quantum hybrid systems using photonic entanglement [1]. The confinement of electromagnetic fields in mesoscopic mode volumes, as in the case of on-chip superconducting cavities, allows the study of light and matter interactions in the strong-coupling regime when the coupling strength g_c exceeds the qubit dephasing rate γ and the cavity dissipation rate κ_c [2]. Experimentally, electric dipole coupling between electromagnetic excitations in a cavity and a single quantum emitter has been achieved in atomic systems [3] and superconducting qubits [4], where the electric dipole interaction with the cavity mode is large. In contrast, achieving strong magnetic coupling between an electromagnetic field and a single quantum spin remains elusive due to its small magnetic dipole. However, the interaction can be collectively enhanced by employing an ensemble of N-identical spins such that the ensemble coupling strength is enhanced by a factor of $\sqrt{N}$. In this way, strong coupling has been demonstrated with various spin systems, such as N-V centers and point defects in diamond [5–7], molecular magnets [8–10], and transition metals and rare-earth (RE) ions in crystals [6,11–15]. Moreover, recent studies using Er^{3+}:Y_2SiO_5 spin-diluted crystals [16], N-V centers in diamond [17], and Bi defects in Si [18] have demonstrated the storage and retrieval of the state of microwave photons at high power and near the quantum limit regime.

Among the $4f$ ions, Gd^{3+} is half filled and possesses the largest spin quantum number ($S = 7/2$) with no orbital angular momentum ($L = 0$). When doped into $CaWO_4$, this spin provides a large magnetic moment and crystal field, which in moderate fields (approximately 0.1 kG) allows spin transitions at large frequencies of approximately 18 GHz. The characteristics of the crystal field allow the use of clock transitions where the spin coherence is insensitive to field fluctuations [19]. It is important to note that the higher the transition (or cavity) frequency, the higher is the spin-photon coupling, which is another benefit of the Gd^{+3} crystal field. Nevertheless, using a frequency regime, the resulting spin dynamics are still practical for integration in circuit quantum electrodynamics (QED) architectures.

*gf15@fsu.edu
†ichiorescu@fsu.edu

 © 2023 American Physical Society

By performing field-dependent cavity-spectroscopy measurements, we explore the coupling between a Gd^{3+} spin ensemble and a superconducting on-chip resonator. We demonstrate that the strong-coupling regime is characterized by a large avoided crossing of 146 MHz, so large that it leads to a significant perturbation of the ground state of the crystal due to the presence of a photon. The experimentally observed spin-cavity dressed states are well described by the Dicke model [20] for a multilevel system with high anisotropy. Moreover, we perform pulsed electron-spin-resonance (ESR) measurements that show a population inversion and suggest a way to perform active cooling of the spin system into its ground state.

II. OBSERVATION OF THE STRONG-COUPLING REGIME DESCRIBED BY THE DICKE MODEL

The spectroscopy of the resonator-photon spin interaction is studied using a home-built heterodyne detector [19]. The sample holder is introduced inside a superconducting vector magnet with field $\mathbf{H}_0$ and thermally anchored to the mixing chamber of a dilution refrigerator at $T \simeq 0.38$ K. The resonator is etched out of a 20-nm Nb film and contains a transition from a coplanar waveguide (CPW) to a coplanar strip line (CPS) [21], matched for a 50-Ω impedance. The CPS is capacitively coupled to a $\lambda/4$ resonant structure that ends with a short circuit shaped into an Ω loop (internal radius of 15 μm). Figure 1(a) shows a single crystal (size $\simeq 2.5 \times 1 \times 0.6$ mm^3) of $CaWO_4$ with a 0.05% spin concentration of Gd^{3+} [Fig. 1(b)] well pressed on a bead of grease atop of the loop, where the field distribution of the resonant mode is mostly concentrated [see Figs. 1(c) and 1(d)]. The crystal has a $I4/a$ tetragonal symmetry with lattice constants of the unit cell $a = b = 5.24$ Å and $c = 11.38$ Å.

The electron-spin Hamiltonian of the Gd^{3+} $S = 7/2$ ion is given by [22,23]

$$\mathscr{H}_s = \mu_B \mathbf{H}_0^T \mathbf{g} \mathbf{S} + B_2^0 O_2^0 + B_4^0 O_4^0 + B_4^4 O_4^4 + B_6^0 O_6^0 + B_6^4 O_6^4, \quad (1)$$

where the O_k^q are the Stevens operators [24], μ_B is the Bohr magneton, $\mathbf{H}_0$ is the applied magnetic field vector, and $(g_\parallel, g_\perp) = (1.991, 1.992)$ are the g factors parallel and perpendicular to the crystallographic c axis, respectively.

Measurements of the field- and frequency-dependent reflected microwave power are given in Fig. 2(a). The spin-resonator system is probed with a long 10-μs pulse at a 5-ms repetition time, to allow spin relaxation before each pulse. The repetition time is on par with relaxation-time measurements done at 6 K [25]. A sequence of 320 pulses is sent and the averaged fast Fourier transform (FFT) of the reflected signal ring down is recorded. At the sample-holder level, we estimate the power to be $P_{\rm in} = -64$ dBm [see Fig. 1(a)]. For a fixed field H_0, the excitation frequency ω is swept around the cavity resonance and the process is repeated from negative to positive H_0 values. A small background signal is recorded away from the spin-cavity resonance and subtracted from the reflected power, in order to remove unwanted resonances attributed to impedance mismatch between the coaxial line and sample holder. A strong hybridization between the spin and cavity modes results in the observed avoided crossing at $H_r \approx \pm 0.072$ kG, where the splitting has the largest value (146 ± 1 MHz). As described below, we use an exact diagonalization and a least-squares algorithm to fit the data and the simulated spectrum is in good agreement with the experimental results [see Fig. 2(b)].

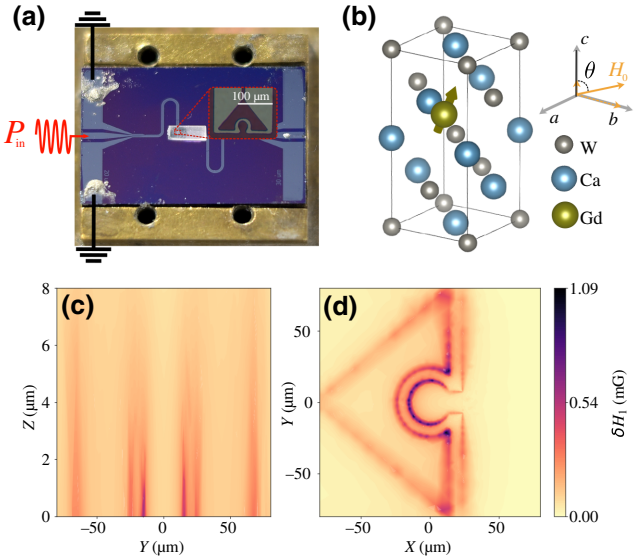

FIG. 1. (a) The coplanar-strip-line resonator with a Gd^{3+} spin sample. The inset shows an optical micrograph of the Ω-shaped short circuit. (b) The unit cell of the Gd^{3+}-doped $CaWO_4$ crystal; the O atoms are removed for clarity. A static field H_0 is applied at an angle $\theta = 81.46°$ relative to the crystallographic c axis. (c),(d) COMSOL simulations of the $\delta H_1^{\rm rms}$-field distribution (the vacuum field corresponding to $P_{\rm rms} = -124.1$ dBm) at (c) the center of the Ω-shaped loop versus the distance z from the chip and (d) at the chip surface $z = 0$, showing where the $\delta H_1^{\rm rms}$ field is mostly concentrated.

Figure 2(c) shows reflected power $P_{11}(\omega/2\pi)$ (in decibel milliwatts) for $\omega_s = \omega_c$, where the two reflection dips have equal intensity and the largest split (ω_s is the spin-level separation and ω_c is the resonator mode). The fit (orange line) of the reflection scattering coefficient is based on input-output formalism in the presence of a spin system [6,26] ($P_{11} \propto S_{11}^2$):

$$|S_{11}|^2(\omega) = \left| 1 + \frac{\kappa_e}{i(\omega - \omega_c) - \kappa_c + \frac{g_c^2}{i(\omega - \omega_s) - \gamma_s}} \right|^2. \quad (2)$$

The cavity $\kappa_c/2\pi = 10.485$ MHz and external $\kappa_e/2\pi \approx 0.99\kappa_c/2\pi = 10.38$ MHz damping rates of the resonator

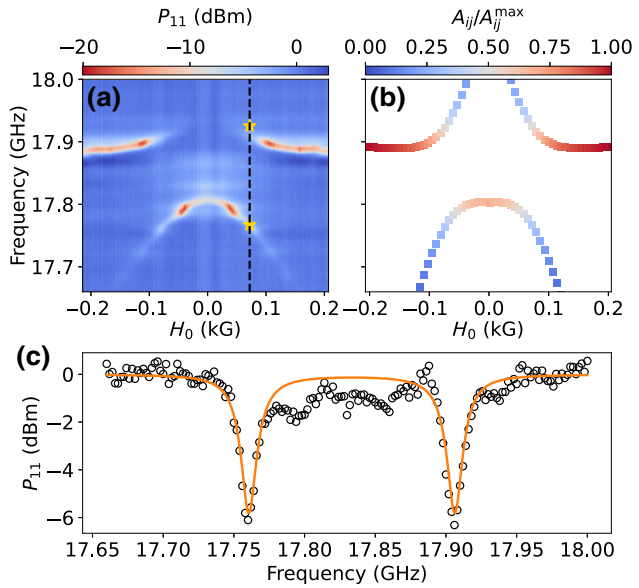

FIG. 2. (a) The reflected power as a function of the field and frequency, showing a large splitting of approximately 146 MHz due to spin-photon strong coupling. The dashed line indicates the location of maximum separation between dips. (b) The normalized $A_{2,4}$ and $A_{2,5}$ values [see Eq. (4)] as the lower and upper branches, respectively. Simulated resonance frequencies are shown by yellow stars in (a), in good agreement with the experiment. (c) The reflected power P_{11} (black circles) at the resonance field represented by the dashed line in (a). The solid orange line corresponds to a fit to the data using Eq. (2).

are determined from the reflected spectrum away from resonance and used as fit constants. We obtain an ensemble spin-resonator coupling strength $g_c/2\pi = 73.0 \pm 0.6$ MHz and a spin line width (dephasing rate) $\gamma_s/2\pi = 8.8 \pm 1.5$ MHz. The g_c value is simply half of the signal splitting and is an oversimplified view when translated to the Gd multilevel system. The coupling term between the Gd^{3+} spin $S = 7/2$ and the photon mode has to be described by the Dicke model [20], initially proposed to describe the superradiance emission of light by an ensemble of N atoms. We apply it here for spin $S = N/2$, with $N = 7$ in the presence of the $CaWO_4$ crystal field:

$$\mathscr{H} = \mathscr{H}_s + \frac{\omega_c}{2\pi} a^\dagger a + \frac{g_c}{2\pi}\left(a^\dagger + a\right)\left(S^+ + S^-\right), \qquad (3)$$

where $a^\dagger$ and a are the photon creation and annihilation operators and the $S_\pm$ are the spin-raising and -lowering operators, respectively.

Contrary to the Tavis-Cumming model, the inclusion of the counter-rotating coupling terms is necessary for spin $S = 7/2$ in the presence of a crystal field, where the zero-field splitting energy is comparable to the resonator transition frequency. As discussed below, the number of photons in the cavity $n_c = a^\dagger a$ is much smaller than the number of excited spins and therefore we can use an exact diagonalization of $\mathscr{H}$ for $n_c = 0, 1$, which is a $2(2S+1)$ matrix. The spin-photon eigenvalues and eigenstates $\{E_k, |k\rangle\}_{k=1\ldots16}$ in the laboratory frame are obtained as a function of the H_0 size and orientation.

In order to reproduce the observed signals, we analyze the $|2\rangle \rightarrow |4\rangle$ and $|2\rangle \rightarrow |5\rangle$ transitions, indicated in Fig. 3 with green and orange arrows, respectively. We compute the absorption spectra, as the ones shown in Fig. 2(b), using the transition amplitude:

$$A_{if} = |\langle\psi_f|a|\psi_i\rangle|^2 e^{-E_i/(k_B T)}\delta\left(E_f - E_i - \hbar\omega\right), \qquad (4)$$

for which a maximum value implies a photon absorption and thus a minimum in the $|S_{11}|^2$. The state $|\psi_i\rangle = |2\rangle$ is the first excited pure spin state; $|\psi_f\rangle = |4\rangle$ and $|\psi_f\rangle = |5\rangle$ correspond to the final states for the lower and upper branch transitions, respectively [Fig. 2(b)]. These states are shown in Table I and obtained by exact diagonalization using the Quantum Toolbox (QuTiP) in PYTHON [27].

An iterative least-squares comparison between the experimental spectra [Fig. 2(a)] and the calculated transition frequencies [Fig. 2(b)] leads to crystal-field parameters B_k^q, a cavity resonance frequency $\omega_c/2\pi$, a relative orientation θ of the static field relative to the c axis, and a spin-cavity coupling strength g_c: $B_2^0 = -945.66$, $B_4^0 = -1.2435$, $B_4^4 = -25.3$, $B_6^0 = 5.712 \times 10^{-4}$, and $B_6^4 = 70.0 \times 10^{-4}$ (all in megahertz); $\omega_c/2\pi = 17930.7$ MHz, $\theta = 81.66^\circ$, and $g_c/2\pi = 57.35$ MHz. All of the crystal-field parameters agree with our previous weak-coupling study [19] to within a 1% difference except for B_4^4, which here is found to be 3.5 times larger.

The six lowest eigenenergies $|k\rangle_{k=1\ldots6}$ are shown in Fig. 3(a) for $g_c/2\pi = 0$ (dashed gray) and $g_c/2\pi = 57.35$ MHz (blue). For $g_c = 0$, the states are labeled $|g, n_c\rangle$ and $|e_j, n_c\rangle$, with $n_c = 0, 1$ for the ground and the jth excited spin state, respectively ($j = 1, 2, 3$). States $|\{g, e_1\}, 0\rangle$ and $|\{e_2, e_3\}, 0\rangle$ correspond to the 7/2 and 5/2 Kramers doublets, respectively (see Fig. 3(b) left), split by the transverse field H_0. States $|\{g, e_1\}, 1\rangle$ correspond to the $|S_z| \cong 7/2$ doublet raised by $\hbar\omega_c$ (see Fig. 3(b) right). A spin-cavity coupling strength $g_c/2\pi = 57.35$ MHz leaves $|1\rangle = |g, 0\rangle$ and $|2\rangle = |e_1, 0\rangle$ untouched but gives a hybridization between the $|e_1, 1\rangle$ and $|e_2, 0\rangle$, leading to the experimentally observed gap of 146 MHz between states $|4\rangle$ and $|5\rangle$ (states $|\{3, 4, 5\}\rangle$ are listed in Table I). Thus, the exact diagonalization leads to a cooperativity factor $C = g_c^2/\kappa_c\gamma_s \approx 35$ rather than approximately 58 obtained from the two-level picture of the S_{11} fit. We note that larger factors have been inferred in other RE ions [15] but no gap is observed.

The observed large difference in the crystal-field B_4^4 parameter between the weak- and strong-coupling cases, as mentioned above, can be explained using the Dicke Hamiltonian of Eq. (3). We calculate the change in $E_1 \cong E_{g,0}$ at zero field as a function of B_4^4 (see Fig. 3(c), left axis) and

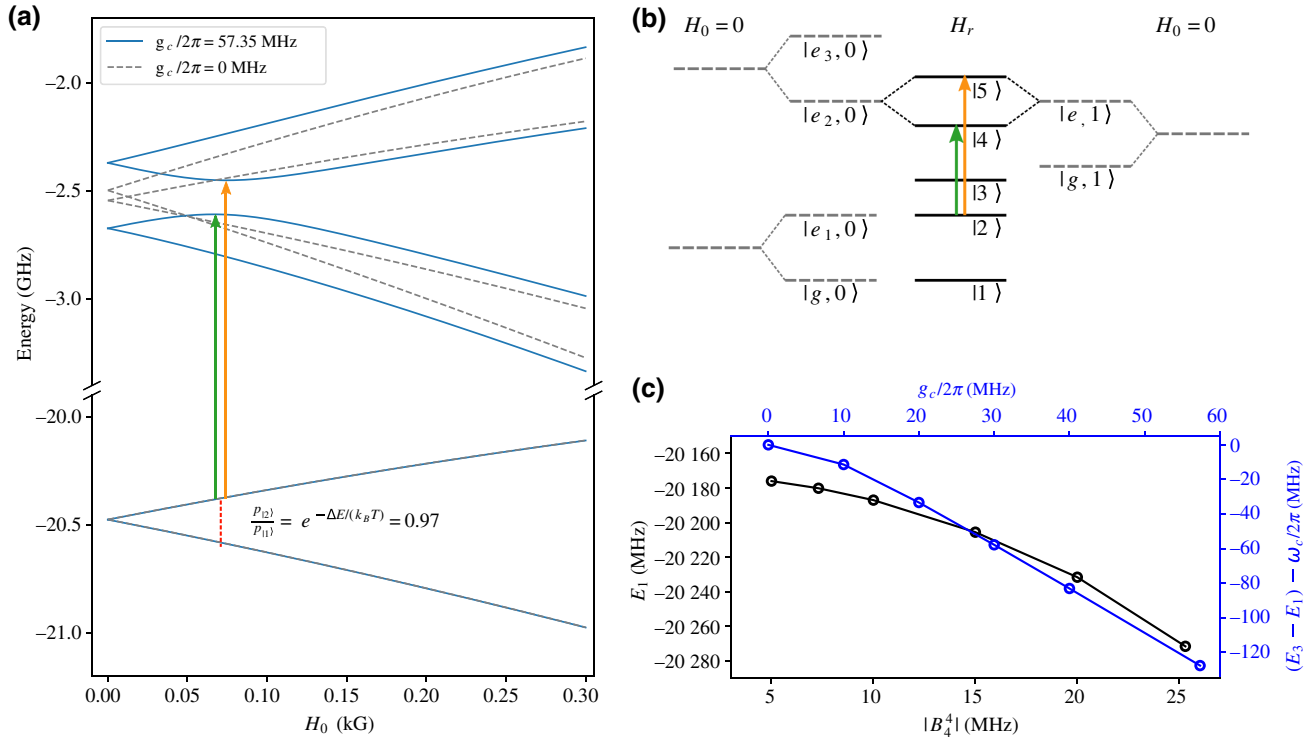

FIG. 3. (a) The lowest six spin-resonator eigenenergies. For $g_c = 0$ (dark gray) the states are pure spin states: ground $|g, 0\rangle$ and excited $|\{e_1, e_2, e_3\}, 0\rangle$ states for zero photons and $|g, 1\rangle$, $|e_1, 1\rangle$ for one photon in the resonator. For a large coupling $g_c/2\pi = 57.35$ MHz (blue lines), a hybridization of $|e_2, 0\rangle$ and $|e_1, 1\rangle$ is indicated by the green and orange arrows. (b) The energy-ladder diagram (not to scale). The $g_c = 0$ states are shown by the dashed gray lines for the cases of zero (left) and one (right) photons. The hybridized states ($g_c > 0$) at resonance are represented by the solid black lines: $|2\rangle \rightarrow |4\rangle$ and $|2\rangle \rightarrow |5\rangle$ correspond to the experimentally observed resonances. (c) The calculated perturbation of the spin-cavity ground state at zero field due to: (i) the crystal-field term B_4^4, with no photons in the cavity (left axis, black squares) and (ii) a single photon in the cavity seen as $(E_3 - E_1) - \omega_c/2\pi$ as a function of $g_c/2\pi$ (right axis, blue dots); the two vertical axes have the same range. The two dependencies are similar, which indicates that the change in B_4^4 is due to the presence of a photon field in the cavity.

compare it to the change brought about by the presence of a single photon in the cavity $E_3 - E_1$ as a function of g_c for fixed $B_4^4 = -25.3$ MHz ($E_3 = E_{g,1}$ only for $g_c = 0$). For a proper comparison, the photon frequency needs to be subtracted as well, as shown in Fig. 3(c) (right axis). The two vertical axes of Fig. 3(c) have the same range: as B_4^4 or g_c increases, so does the perturbation of the electronic ground state, leading to an approximately 130 MHz shift for the measured values of B_4^4 and g_c. The similarity between the two trends indicates that the photon field is so

TABLE I. The eigenstates of the cavity-spin Hamiltonian at the observed resonance field $H_r = 72$ G. Amplitude coefficients less than 0.01 have been disregarded for clarity.

$\|3\rangle =$	$S_z = 7/2$	$S_z = 5/2$	$S_z = 3/2$	$S_z = 1/2$	$S_z = -1/2$	$S_z = -3/2$	$S_z - 5/2$	$S_z = -7/2$
$n = 0$	0.010	−0.629	−0.092	0	0	−0.153	−0.318	0
$n = 1$	0.669	0.01	0	0	0.036	0	0	0.145
$\|4\rangle =$	$S_z = 7/2$	$S_z = 5/2$	$S_z = 3/2$	$S_z = 1/2$	$S_z = -1/2$	$S_z = -3/2$	$S_z - 5/2$	$S_z = -7/2$
$n = 0$	0	0.145	0.140	0	0	0.05	0.578	0
$n = 1$	0.561	0	0	−0.03	0.03	0	0	−0.553
$5\rangle =$	$S_z = 7/2$	$S_z = 5/2$	$S_z = 3/2$	$S_z = 1/2$	$S_z = -1/2$	$S_z = -3/2$	$S_z = -5/2$	$S_z = -7/2$
$n = 0$	0	0.605	0.015	0	0	0.141	−0.010	0
$n = 1$	0.460	0	0	0.033	0.024	0	0	0.631

strongly coupled to spin that the electrostatic interaction, intrinsic to the crystal only, is severely perturbed.

III. ESTIMATION OF SINGLE-SPIN COUPLING STRENGTH

The average single-spin coupling to the resonator is calculated by integrating the coupling to the vacuum field $\delta\mathbf{H}_1$ over the mode volume for an input power $P_{n=0} = \hbar\omega_c\kappa_c/2 = -124.1$ dBm. For $|\psi_{i,f}\rangle = |e_{1,2}, 0\rangle$, the single-spin coupling strength is $g_0(\mathbf{r}) = \gamma_e|\langle\psi_f|\delta\mathbf{H_1}(\mathbf{r})\cdot\mathbf{S}|\psi_i\rangle|$, where $\gamma_e = 2.8025$ MHz/G and $\delta\mathbf{H}_1(\mathbf{r})$ is the spatial distribution of the vacuum fluctuations obtained from the COMSOL finite-element calculations as shown in Figs. 1(c) and 1(d). With a static field approximately perpendicular to the c axis, the leading contribution to g_0 comes from $\langle e_2, 0|S_x|e_1, 0\rangle = 0.715$, while $\langle e_2, 0|S_z|e_1, 0\rangle$ is only 0.01 (calculated using QuTiP) despite the fact that the z-field $\delta H_{1,z}$ contribution is approximately 67% larger than that for $\delta H_{1,x}$ (from COMSOL). The spin-ensemble coupling strength is [19]

$$g_c = \gamma_e\,|\langle e_2, 0|S_x|e_1, 0\rangle|\sqrt{\rho(0.7)\int_{V_m} d^3\mathbf{r}\,\left|\delta H_{1,x}(\mathbf{r})\right|^2}, \quad (5)$$

where V_m is the mode volume, the spin concentration ρ is corrected by $\min(\kappa_c/\gamma_s, 1) = 1$ (spin selectivity as done by the cavity) and for the 70% abundance of the Gd $I = 0$ isotopes.

Assuming no gap between the crystal and the chip, the integration volume V_m is increased around the center of the Ω loop and for $V_m \approx 10^4$ μm^3 (much less than the crystal volume) the experimental value of g_c is obtained (for a similar calculation, see also Ref. [19]); this volume corresponds to $N_s = 7.5\times10^9$ excited spins. Therefore the spatially averaged single-spin coupling strength is $g_0/2\pi = g_c/(2\pi\sqrt{N_s}) \approx 620$ Hz. An upper limit of the number of intraresonator photons can be estimated from the input power at the sample-holder level $P_{\rm in} = -64$ dBm as $n_c = P_{\rm in}/(\hbar\omega_c\kappa_c) = 3.2\times10^6$, thus fulfilling the limit $n_c \ll N_s$.

IV. PULSED ESR WITH DRESSED STATES

In our experiments, we excite state $|2\rangle$ rather than the ground state $|1\rangle$ due to the limited cavity bandwidth and matching between the resonance frequency and spin states. Both states are similar in the sense that they are spin states for $n_c = 0$. We perform pulsed-ESR measurements to study the dynamics of the $|2\rangle \to |4\rangle$ transition and explore a potential way of initializing the system in the $|1\rangle$ ground state. The spin-cavity system is initially in thermal equilibrium at T, with spins almost equally distributed between the $|1\rangle$ and $|2\rangle$ states ($p_{|2\rangle}/p_{|1\rangle} = e^{-\Delta E/(k_BT)} = 0.97, \Delta E = 203$ MHz). A pulse $\omega/2\pi = 17760$ MHz $\cong E_4 - E_2$ [green arrow in Fig. 3(a)] of variable duration τ and power $P_{\rm in}$ is sent to the sample and the FFT of the reflected cavity ring down is analyzed [8,28]. For each

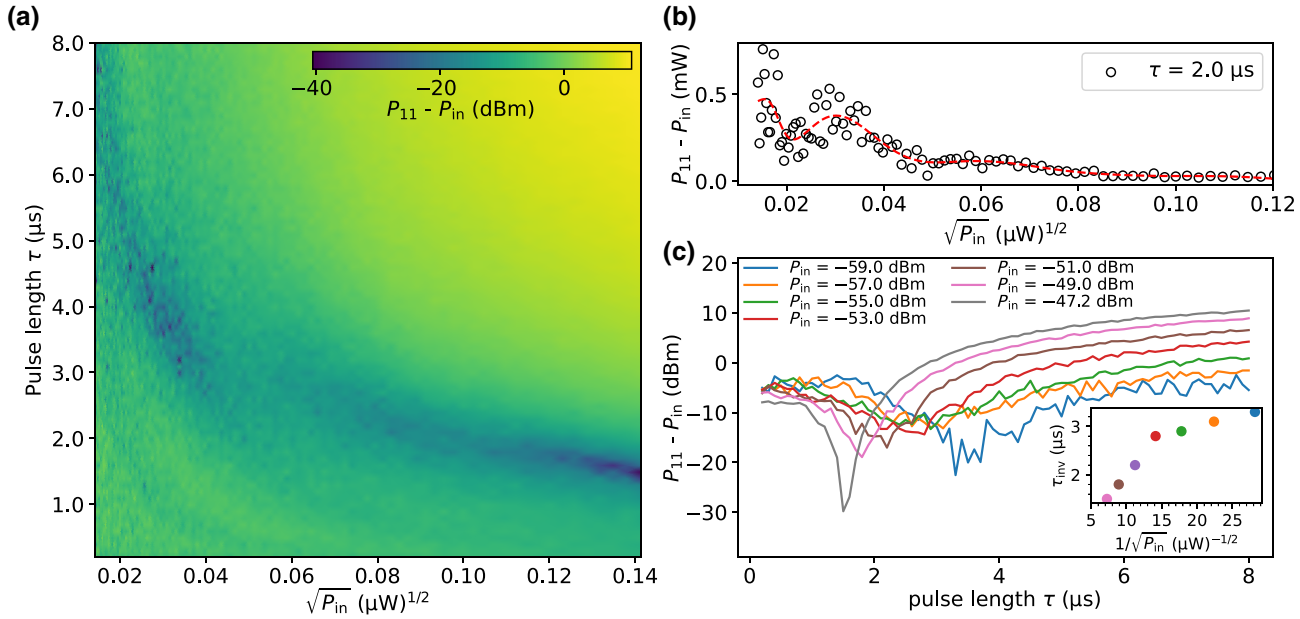

FIG. 4. (a) Pulsed-ESR measurements of the reflected cavity ring-down signal as a function of the pulse length and the square root of the applied drive power. (b) A horizontal cut of the FFT amplitude for a 2-μs pulse and its low-pass FFT average done to remove unwanted noise: a clear pattern corresponding to the Rabi oscillations of the state admixture is seen. (c) Pulse-length cuts of the relative FFT amplitude obtained from (a) at large applied powers $P_{\rm in}$. The inset shows the inversion-pulse length $\tau_{\rm inv}$ versus the inverse of the cavity input drive power $1/\sqrt{P_{\rm in}}$.

power value from $P_{\text{in}} = -67$ dBm to -47 dBm, τ is varied from 0.2 to 8 μs. In Fig. 4(a), the reflected signal $P_{11} - P_{\text{in}}$ is plotted as a function of τ and $\sqrt{P_{\text{in}}}$. P_{in} is subtracted from P_{11} to show that the initial signal ($\tau \to 0$) is the same for all powers. A clear minimum is observed (blue shading), while the other oscillatory features are more vague but present nevertheless.

This aspect is shown better in Fig. 4(b) using the smoothing (dashed red line) of a horizontal cut at constant pulse length $\tau = 2.0$ μs, which indicates a clear damped oscillation of the cavity-spin states. The main minimum is well developed at high powers, as shown by the vertical cuts in Fig. 3(c). The inset shows the position of the dip τ_{inv} as a function of $1/\sqrt{P_{\text{in}}}$ and gives the required pulse length to transfer the population of $|2\rangle$ to $|4\rangle$. In the simplest case of a driven two-level qubit, it is expected that the nutation angle increases linearly with $\sqrt{P_{\text{in}}}$ giving an oscillatory decay of the Rabi signal. In a similar fashion, the inversion time of the Rabi flop will decrease with increasing field amplitude. In the case of our experiments, the Gd spins are multilevel systems in the presence of a large and highly anisotropic crystal field (analyzing the spin dynamics would require solving the time dependence of the full Hamiltonian in the laboratory frame). An outcome of the observed population inversion suggests the possibility of an active cooling procedure [29,30]: (i) a τ_{inv} pulse depletes $|2\rangle$ and populates $|4\rangle$ and (ii) a fast relaxation from $|4\rangle$ to $|1\rangle$ provides the cooling to the ground state. Such relaxation can be induced by a ω_{41} pulse resonant with the $|4\rangle \to |1\rangle$ transition or simply by waiting a certain amount of time. Although ω_{41} is slightly detuned from ω_c, the pulse can have enough power to stimulate the $|4\rangle \to |1\rangle$ transition, by adding another microwave source. Using Eq. (4), we find $A_{24}, A_{41} \gg A_{12} \cong 0$ and thus the relaxation to $|1\rangle$ can take place prior to a repopulation of $|2\rangle$. By repeating the pulse sequence, one can in principle provide a spin initialization in its ground state.

The on-chip pulsed-ESR measurements shown here represent a first step for the characterization of the spin dynamics of this multilevel system. Having a well-known description of the pulse lengths and drive power will lead to π-pulse dynamical decoupling sequences such as spin echo [31] and Carr-Purcell-Meiboom-Gill (CPMG) [32,33] that provide a direct measure of the spin dephasing time.

V. CONCLUSION

In conclusion, we demonstrate the strong-coupling regime between the Gd^{3+} multilevel spin system and an on-chip superconducting resonator. Using exact diagonalization of the spin-cavity Dicke Hamiltonian, we estimate the coupling strength of the spin ensemble as $g_c/2\pi = 57.35$ MHz. Together with the estimated cavity and spin dephasing rates, this leads to a cooperativity factor $C \approx 35$ and an averaged single-spin coupling strength of 620 Hz. The dynamics of the cavity-spin states are explored using pulsed-ESR measurements and a population inversion is observed. Most remarkably, we measure a strong perturbation of the anisotropic crystal-field parameter B_4^4 due to the large coupling between the spins and the resonator.

ACKNOWLEDGMENTS

This work was performed at the National High Magnetic Field Laboratory (NHMFL) at Florida State University (FSU) and supported by the National Science Foundation through Grant No. NSF/DMR-1644779 and the State of Florida. We acknowledge discussions with Dr. Petru Andrei (FSU) and we thank Dr. A.M. Tkachuk for providing the sample. S.B. acknowledges support from CNRS research infrastructure INFRANALYTICS (FR2054) and the International Emerging Action QUantum Dynamics at ultra Low Temperature (QULT). S.M. acknowledges support from Grants-in-Aid for Scientific Research C (Grant No. 18K03444) and the Elements Strategy Initiative Center for Magnetic Materials (ESICMM) funded by the Ministry of Education, Culture, Sports, Science, and Technology (MEXT) of Japan (Grant No. 12016013).

[1] G. Kurizki, P. Bertet, Y. Kubo, K. Mølmer, D. Petrosyan, P. Rabl, and J. Schmiedmayer, Quantum technologies with hybrid systems, Proc. Nat. Acad. Sci. **112**, 3866 (2015).

[2] S. Haroche and J.-M. Raimond, *Exploring the Quantum* (Oxford University Press, New York, 2006).

[3] R. J. Thompson, G. Rempe, and H. J. Kimble, Observation of Normal-Mode Splitting for an Atom in an Optical Cavity, Phys. Rev. Lett. **68**, 1132 (1992).

[4] A. Wallraff, D. I. Schuster, A. Blais, L. Frunzio, R.-S. Huang, J. Majer, S. Kumar, S. M. Girvin, and R. J. Schoelkopf, Strong coupling of a single photon to a superconducting qubit using circuit quantum electrodynamics, Nature **431**, 162 (2004).

[5] Y. Kubo, F. R. Ong, P. Bertet, D. Vion, V. Jacques, D. Zheng, A. Dréau, J. F. Roch, A. Auffeves, F. Jelezko, J. Wrachtrup, M. F. Barthe, P. Bergonzo, and D. Esteve, Strong Coupling of a Spin Ensemble to a Superconducting Resonator, Phys. Rev. Lett. **105**, 140502 (2010).

[6] D. I. Schuster, A. P. Sears, E. Ginossar, L. Dicarlo, L. Frunzio, J. J. L. Morton, H. Wu, G. A. D. Briggs, B. B. Buckley, D. D. Awschalom, and R. J. Schoelkopf, High-Cooperativity Coupling of Electron-Spin Ensembles to Superconducting Cavities, Phys. Rev. Lett. **105**, 140501 (2010).

[7] R. Amsüss, C. Koller, T. Nöbauer, S. Putz, S. Rotter, K. Sandner, S. Schneider, M. Schramböck, G. Steinhauser, H. Ritsch, J. Schmiedmayer, and J. Majer, Cavity QED with Magnetically Coupled Collective Spin States, Phys. Rev. Lett. **107**, 060502 (2011).

[8] I. Chiorescu, N. Groll, S. Bertaina, T. Mori, and S. Miyashita, Magnetic strong coupling in a spin-photon system and transition to classical regime, Phys. Rev. B **82**, 024413 (2010).
[9] A. Eddins, C. Beedle, D. Hendrickson, and J. R. Friedman, Collective Coupling of a Macroscopic Number of Single-Molecule Magnets with a Microwave Cavity Mode, Phys. Rev. Lett. **112**, 120501 (2014).
[10] C. Bonizzoni, A. Ghirri, and M. Affronte, Coherent coupling of molecular spins with microwave photons in planar superconducting resonators, Adv. Phys.: X **3**, 1435305 (2018).
[11] P. Bushev, A. K. Feofanov, H. Rotzinger, I. Protopopov, J. H. Cole, C. M. Wilson, G. Fischer, A. Lukashenko, and A. V. Ustinov, Ultralow-power spectroscopy of a rare-earth spin ensemble using a superconducting resonator, Phys. Rev. B **84**, 060501(R) (2011).
[12] S. Probst, H. Rotzinger, S. Wünsch, P. Jung, M. Jerger, M. Siegel, A. V. Ustinov, and P. A. Bushev, Anisotropic Rare-Earth Spin Ensemble Strongly Coupled to a Superconducting Resonator, Phys. Rev. Lett. **110**, 157001 (2013).
[13] A. K. V. Keyser, J. J. Burnett, S. E. Kubatkin, A. V. Danilov, M. Oxborrow, S. E. d. Graaf, and T. Lindström, Pulsed electron spin resonance of an organic microcrystal by dispersive readout, J. Magn. Reson. **321**, 106853 (2020).
[14] G. Dold, C. W. Zollitsch, J. O'Sullivan, S. Welinski, A. Ferrier, P. Goldner, S. de Graaf, T. Lindström, and J. J. Morton, High-Cooperativity Coupling of a Rare-Earth Spin Ensemble to a Superconducting Resonator Using Yttrium Orthosilicate as a Substrate, Phys. Rev. Appl. **11**, 054082 (2019).
[15] S. Wang, L. Yang, R. L. Cone, C. W. Thiel, and H. X. Tang, High-Cooperativity Coupling of Rare-Earth Spins to a Planar Superconducting Resonator, Phys. Rev. Appl. **18**, 014071 (2022).
[16] S. Probst, H. Rotzinger, A. V. Ustinov, and P. A. Bushev, Microwave multimode memory with an erbium spin ensemble, Phys. Rev. B **92**, 014421 (2015).
[17] C. Grezes, B. Julsgaard, Y. Kubo, W. L. Ma, M. Stern, A. Bienfait, K. Nakamura, J. Isoya, S. Onoda, T. Ohshima, V. Jacques, D. Vion, D. Esteve, R. B. Liu, K. Mølmer, and P. Bertet, Storage and retrieval of microwave fields at the single-photon level in a spin ensemble, Phys. Rev. A **92**, 020301(R) (2015).
[18] V. Ranjan, J. O'Sullivan, E. Albertinale, B. Albanese, T. Chanelière, T. Schenkel, D. Vion, D. Esteve, E. Flurin, J. J. L. Morton, and P. Bertet, Multimode Storage of Quantum Microwave Fields in Electron Spins over 100 ms, Phys. Rev. Lett. **125**, 210505 (2020).
[19] G. Franco-Rivera, J. Cochran, L. Chen, S. Bertaina, and I. Chiorescu, On-Chip Detection of Electronuclear Transitions in the ^{155,157}Gd Multilevel Spin System, Phys. Rev. Appl. **18**, 014054 (2022).
[20] R. H. Dicke, Coherence in spontaneous radiation processes, Phys. Rev. **93**, 99 (1954).
[21] D. E. Anagnostou, M. Morton, J. Papapolymerou, and C. G. Christodoulou, A 0–55 GHz coplanar waveguide to coplanar strip transition, IEEE Trans. Microw. Theory Tech. **56**, 1 (2008).
[22] C. F. Hempstead and K. D. Bowers, Paramagnetic resonance of impurities in $CaWO_4$. I. Two *s*-state ions, Phys. Rev. **118**, 131 (1960).
[23] A. Zalkin and D. H. Templeton, X-ray diffraction refinement of the calcium tungstate structure, J. Chem. Phys. **40**, 501 (1964).
[24] C. Rudowicz and C. Y. Chung, The generalization of the extended Stevens operators to higher ranks and spins, and a systematic review of the tables of the tensor operators and their matrix elements, J. Phys.: Condens. Matter **16**, 5825 (2004).
[25] E. I. Baibekov, M. R. Gafurov, D. G. Zverev, I. N. Kurkin, A. A. Rodionov, B. Z. Malkin, and B. Barbara, Coherent spin dynamics in a gadolinium-doped $CaWO_4$ crystal, Phys. Rev. B **95**, 064427 (2017).
[26] E. Abe, H. Wu, A. Ardavan, and J. J. L. Morton, Electron spin ensemble strongly coupled to a three-dimensional microwave cavity, Appl. Phys. Lett. **98**, 251108 (2011).
[27] J. Johansson, P. Nation, and F. Nori, Qutip: An open-source PYTHON framework for the dynamics of open quantum systems, Comput. Phys. Commun. **183**, 1760 (2012).
[28] A. Schweiger, *Principles of Pulse Electron Paramagnetic Resonance* (Oxford University Press, Oxford, New York, 2001).
[29] S. O. Valenzuela, W. D. Oliver, D. M. Berns, K. K. Berggren, L. S. Levitov, and T. P. Orlando, Microwave-induced cooling of a superconducting qubit, Science **314**, 1589 (2006).
[30] D. Leibfried, R. Blatt, C. Monroe, and D. Wineland, Quantum dynamics of single trapped ions, Rev. Mod. Phys. **75**, 281 (2003).
[31] E. L. Hahn, Spin echoes, Phys. Rev. **80**, 580 (1950).
[32] H. Y. Carr and E. M. Purcell, Effects of diffusion on free precession in nuclear magnetic resonance experiments, Phys. Rev. **94**, 630 (1954).
[33] S. Meiboom and D. Gill, Modified spin-echo method for measuring nuclear relaxation times, Rev. Sci. Instrum. **29**, 688 (1958).